Supporting Information for:

Investigation on the Interconversion from DMF Solvated to Unsolvated Copper(II) Pyrazolate Coordination Polymers

Corrado Di Nicola,[a,] Alessia Tombesi,[a] Marco Moroni,[b] Rebecca Vismara,[b] Fabio Marchetti,[a] Riccardo Pettinari,[c] Luca Nardo,[b] Guglielmo Vesco,[b] Simona Galli,[b,]* Silvia Casassa,[d] Luciano Pandolfo,[e,]* Claudio Pettinari[c]*

[a] School of Science and Technology, University of Camerino Via S. Agostino 1, 62032 Camerino (MC), Italy.

[b] Dipartimento di Scienza e Alta Tecnologia, Università dell'Insubria, Via Valleggio 11, 22100 Como, Italy.

[c] School of Farmacy, University of Camerino, Via S. Agostino 1, 62032 Camerino (MC), Italy.

[d] Department of Chemistry, University of Turin, and Nanostructured Interfaces and Surfaces Center of Excellence, Via P. Giuria 5, 10125 Torino, Italy.

[e] Department of Chemical Sciences, University of Padova, Via Marzolo 1, 35131 Padova, Italy.

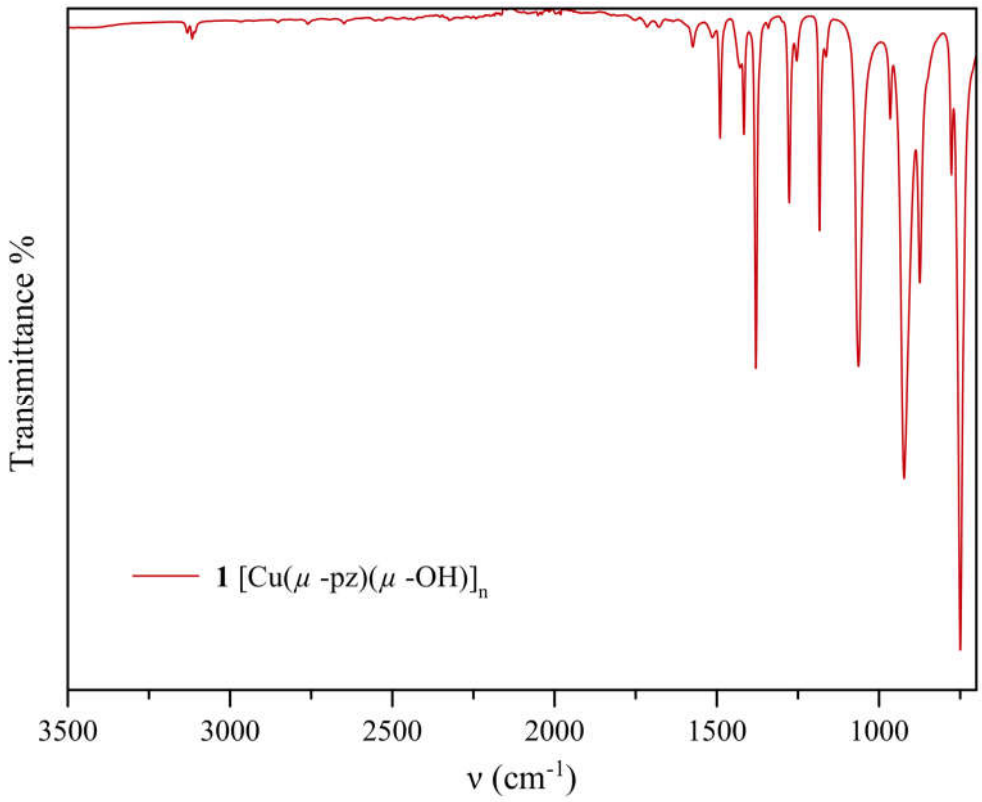

Figure S1. IR spectrum of $[Cu(\mu\text{-pz})(\mu\text{-OH})]_n$ (**1**).

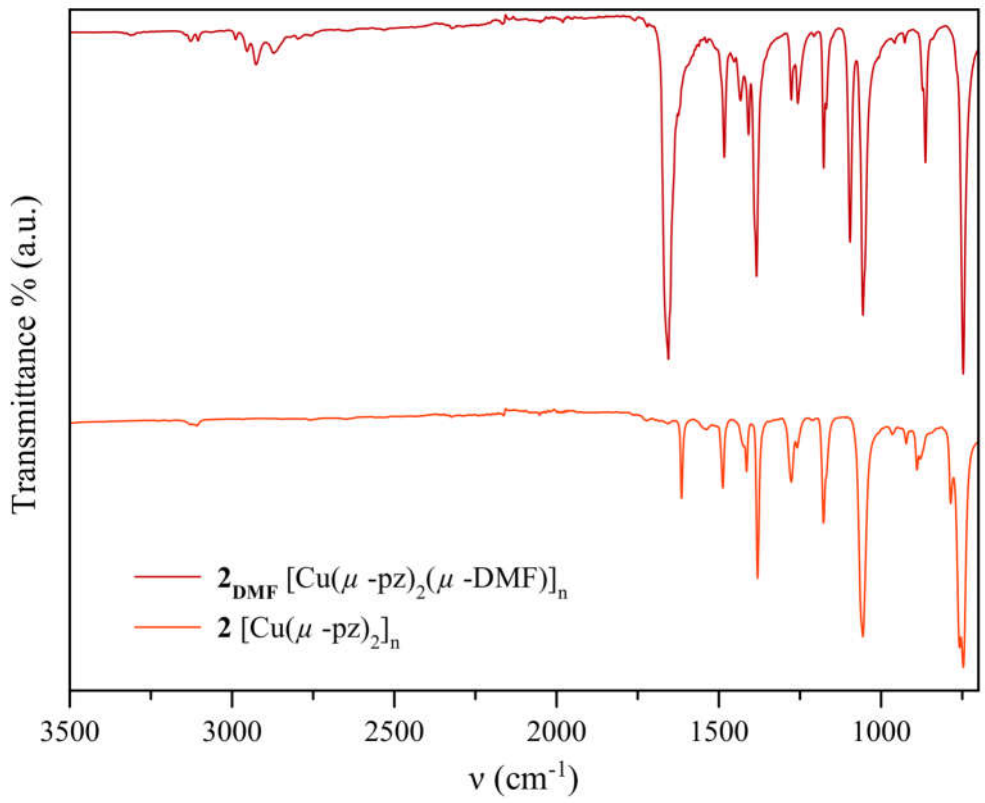

Figure S2. IR spectra of compounds $[Cu(\mu\text{-pz})_2(\mu\text{-DMF})]_n$ (**2**$_{DMF}$, dark red) and $[Cu(\mu\text{-pz})_2]_n$ (**2**, red).

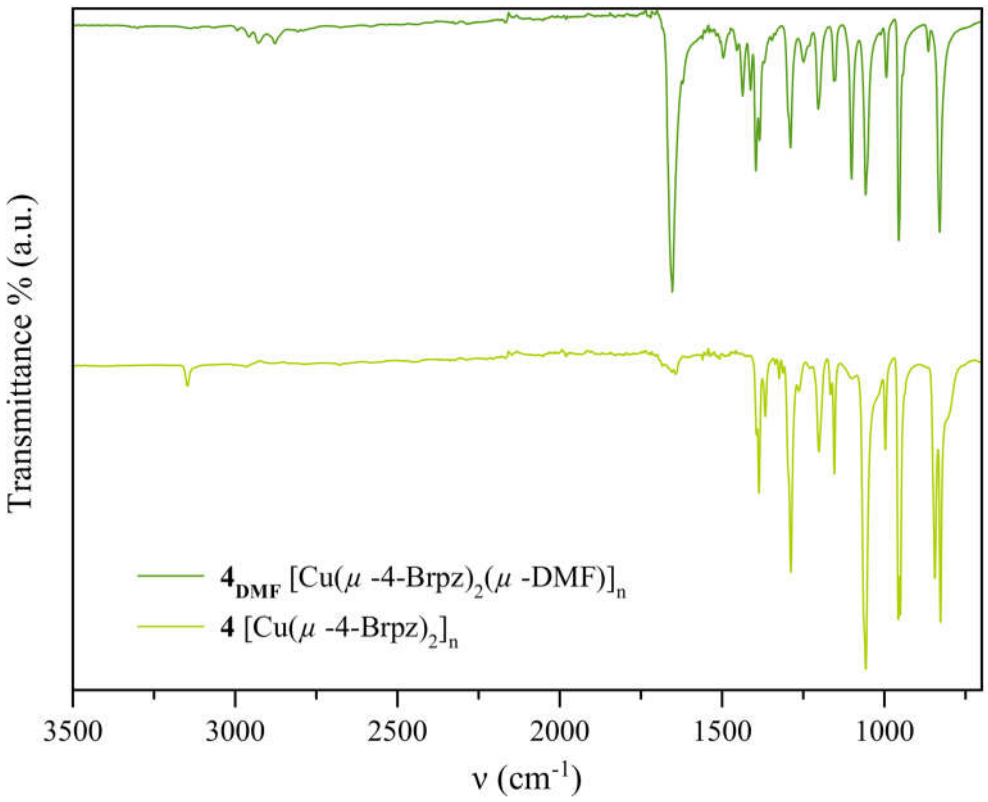

Figure S3. IR spectra of compounds $[Cu(\mu\text{-4-Brpz})_2(\mu\text{-DMF})]_n$ (**4**$_{DMF}$, green) and $[Cu(\mu\text{-4-Brpz})_2]_n$ (**4**, light green).

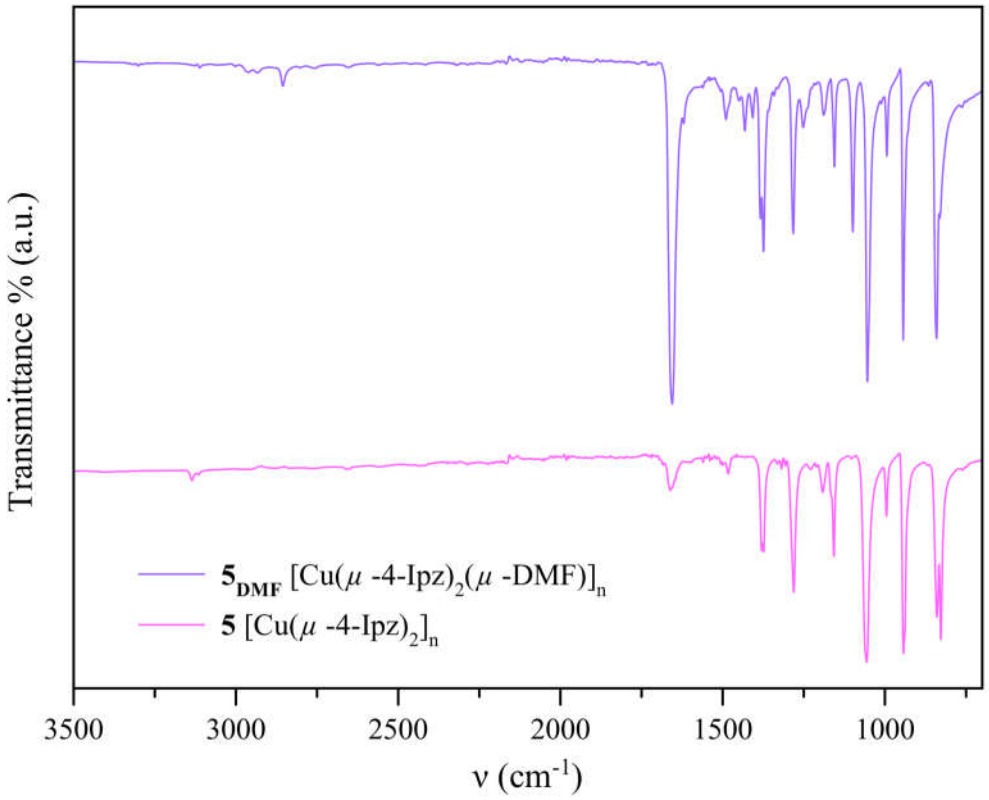

Figure S4. IR spectra of compounds $[Cu(\mu\text{-4-Ipz})_2(\mu\text{-DMF})]_n$ (**5**$_{\mathbf{DMF}}$, violet) and $[Cu(\mu\text{-4-Ipz})_2]_n$ (**5**, fuchsia).

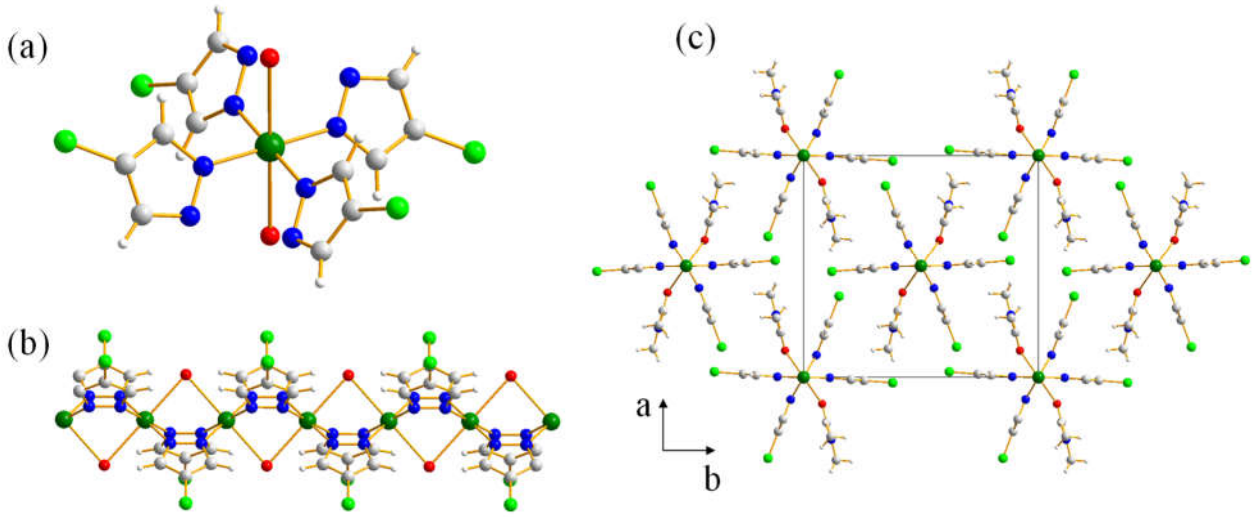

Figure S5. (a) Representation of the *trans*-CuN_4O_2 octahedral stereochemistry of the copper(II) ion in **3**$_{DMF}$. (b) Representation of portion of the 1-D helix of collinear metal ions running along the [001] crystallographic direction in **3**$_{DMF}$. (c) Representation of portion of the crystal packing of **3**$_{DMF}$ viewed along the [001] crystallographic direction. Colour code: Carbon, grey; hydrogen, light grey; chlorine, light green; copper, green; nitrogen, blue; oxygen, red. Main bond distances (Å) and angles (°) at the metal ion: Cu-N 1.923(8), 1.953(9); Cu-O 2.681(9); intra-chain Cu···Cu 3.5692(1); N-Cu-N 89.50(23), 90.50(23), 180; O-Cu-O 180; N-Cu-O 82.99(30)-97.01(30).

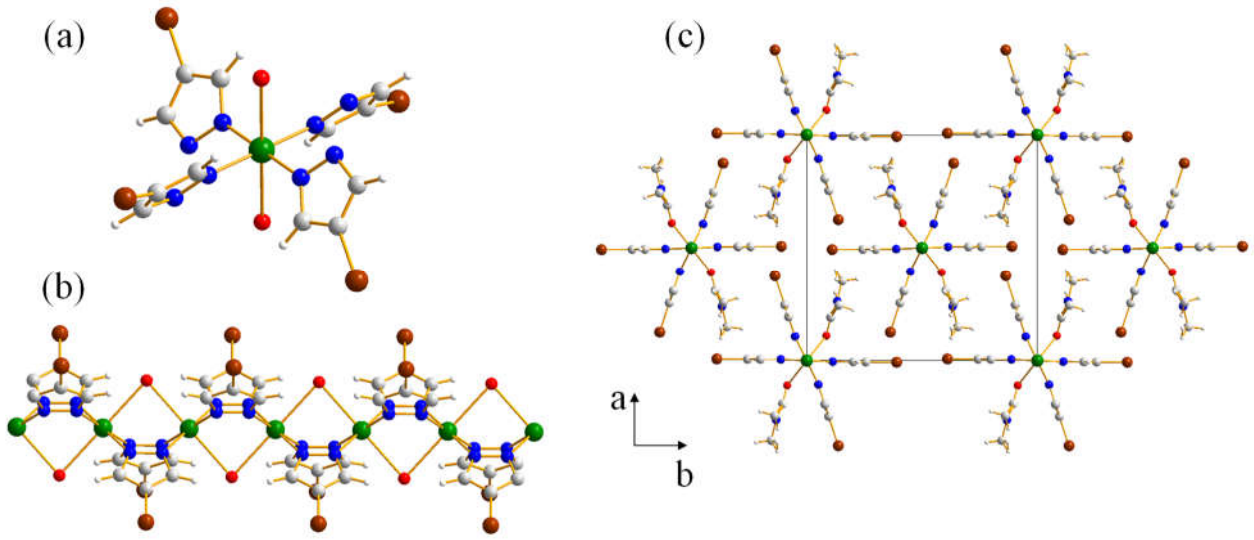

Figure S6. (a) Representation of the *trans*-CuN_4O_2 octahedral stereochemistry of the copper(II) ion in **4**$_{DMF}$. (b) Representation of portion of the 1-D helix of collinear metal ions running along the [001] crystallographic direction in **4**$_{DMF}$. (c) Representation of portion of the crystal packing of **4**$_{DMF}$ viewed along the [001] crystallographic direction. Colour code: Carbon, grey; hydrogen, light grey; bromine, brown; copper, green; nitrogen, blue; oxygen, red. Main bond distances (Å) and angles (°) at the metal ion: Cu-N 1.964(7), 1.999(6); Cu-O 2.656(7); intra-chain Cu···Cu 3.5639(1); N-Cu-N 89.23(16), 90.77(16), 180; O-Cu-O 180; N-Cu-O 84.10(23)-95.90(23).

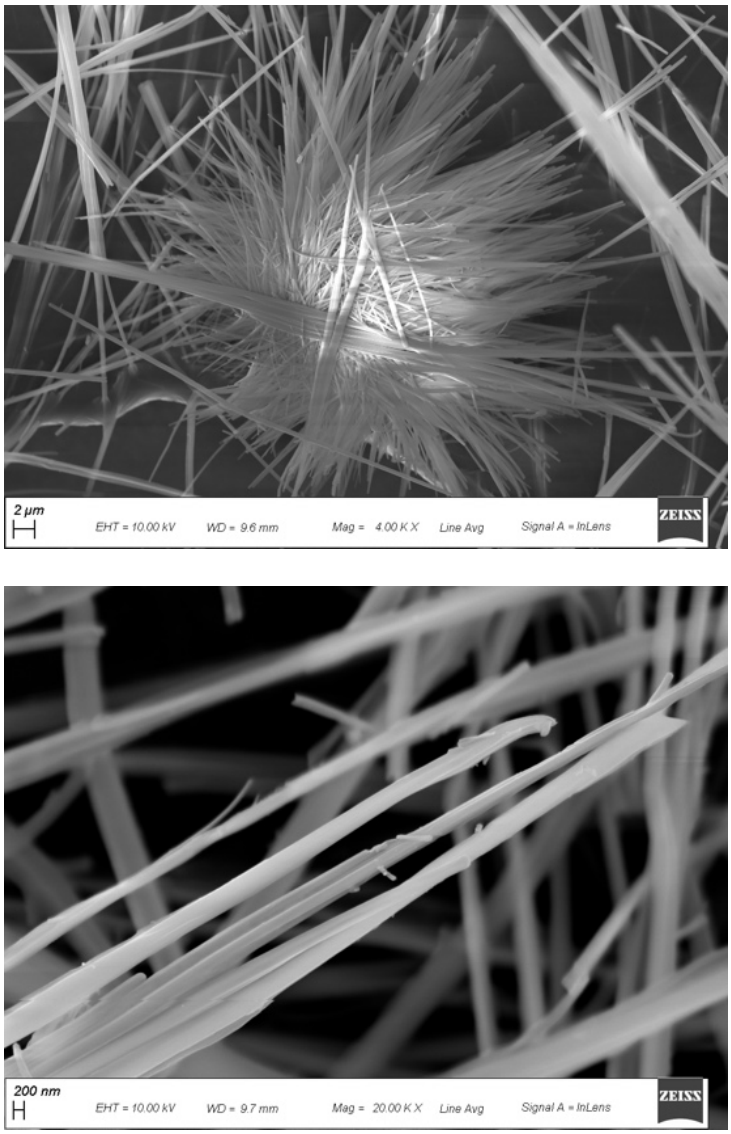

Figure S7. Scanning electron micrographs of a powdered batch of $\mathbf{2_{DMF}}$.

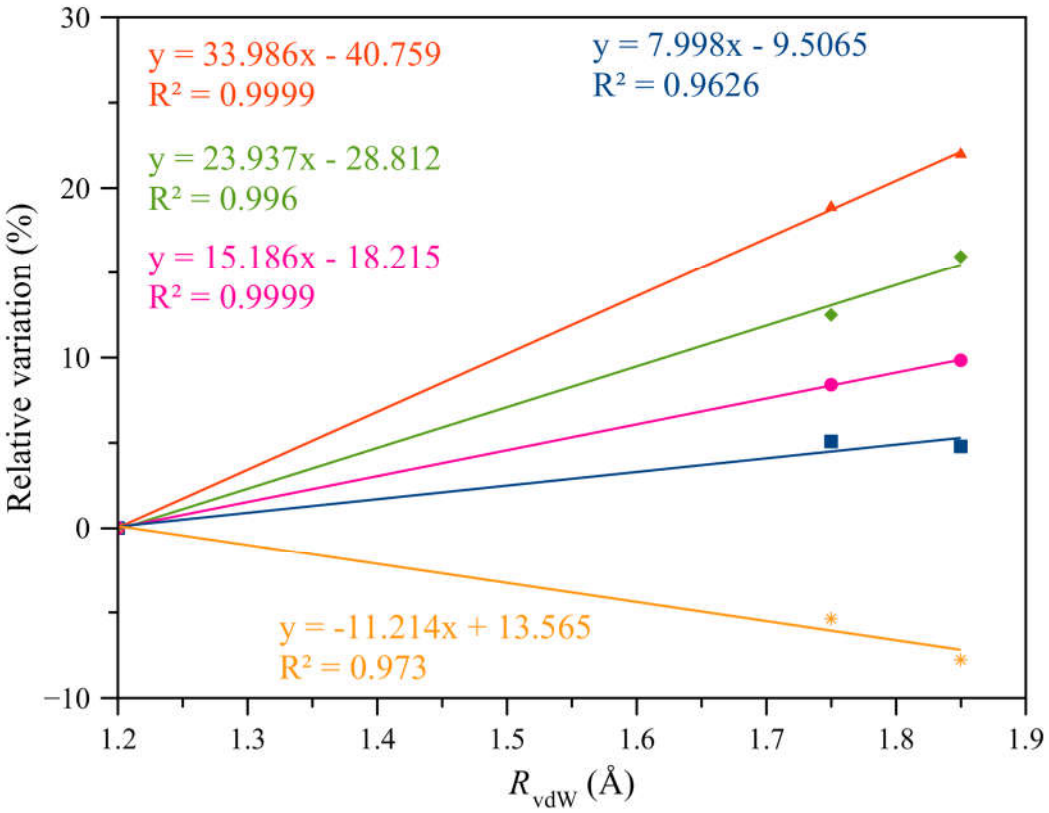

Figure S8. Percentage relative variation of the *a*- (green diamonds) and *b*-axis (blue squares), unit cell volume (red triangles), diagonal of the *C* face (fuchsia circles), atomic packing factor (orange stars) as a function of the van der Waals radii[1] (R_{vdW}) of the atom in position 4 of the pyrazolate ligand in **2**$_{DMF}$-**4**$_{DMF}$. For the calculation of the atomic packing factor, see note *a* of Table S1.

Table S1. van der Waals radii[1] of the atom in position 4 of the pyrazolate ring (R_{vdW}), unit cell parameters, edge of the rhombic motif (e_{rhombi}, half of the diagonal of the *C* face in **2**$_{DMF}$-**4**$_{DMF}$) defined by the reciprocal disposition of the 1-D helices (Figures 4, 5, S5 and S6), and atomic packing factor (APF) in **2**$_{DMF}$-**5**$_{DMF}$.

Compound	R_{vdW} (Å)	*a* (Å)	*b* (Å)	*c* (Å)	e_{rombi} (Å)	APF[a]
2$_{DMF}$	1.20	12.1799(5)	13.7527(6)	7.0999(4)	9.1854(5)	0.97
3$_{DMF}$	1.75	13.7038(3)	14.4516(3)	7.1384(2)	9.9580(3)	0.92
4$_{DMF}$	1.85	14.1228(4)	14.4113(3)	7.1279(2)	10.0888(3)	0.89
oC-5$_{DMF}$	1.98	20.2680(5)	9.5313(2)	7.3586(1)	11.1986(3)	0.91
oP-5$_{DMF}$	1.98	20.1715(4)	9.2333(2)	7.2913(1)	11.0922(2)	0.82

[a] The atomic packing factor has been estimated as the ratio *V*(atoms in the unit cell)/*V*(unit cell), neglecting the contribution of the hydrogen atoms and assigning, to the other atoms, an average volume of 18 Å^3.[2]

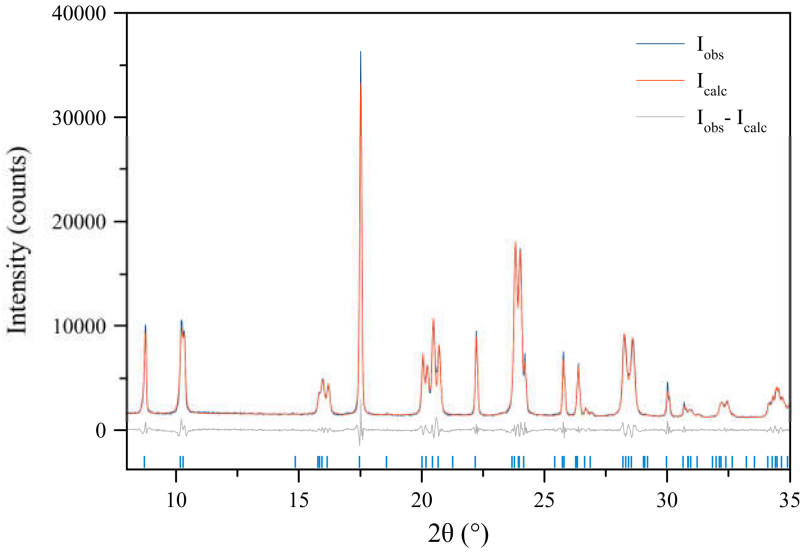

Figure S9. Graphical result of the whole powder pattern refinement carried out with the Le Bail approach on the PXRD pattern of the monoclinic phase of **5DMF** (**m-5DMF**). Experimental, calculated and difference profiles: blue, red and grey, respectively. Peak maxima positions: blue ticks. R_p = 4.01; R_{wp} = 5.26.

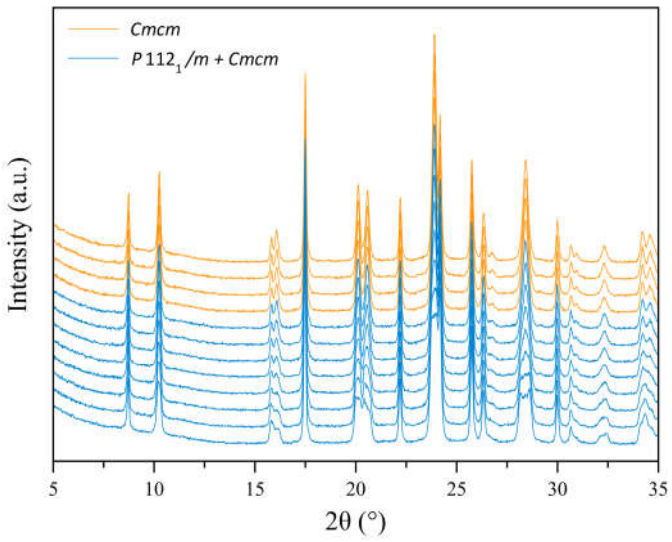

Figure S10. PXRD patterns acquired, as a function of time, starting form a sample of **5DMF** which is a mixture of monoclinic *P* (**m-5DMF**) and orthorhombic *C* (**oC-5DMF**) phases. Blue patterns: mixture of the two phases; orange patterns: orthorhombic *C* phase.

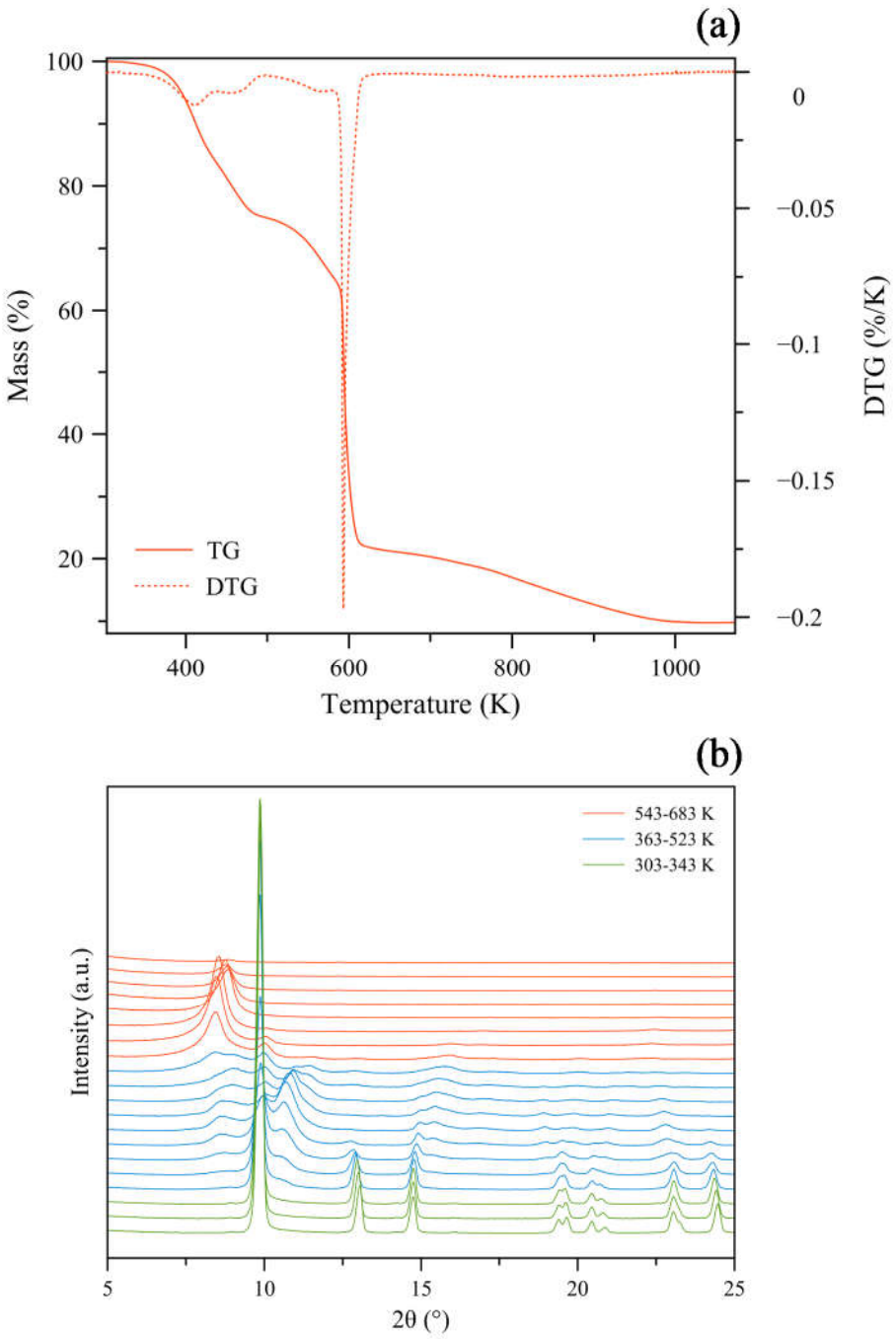

Figure S11. (a) TGA trace (red continuous line) measured under a flow of N_2 on **2**$_{DMF}$ and the corresponding DTG trace (red dashed line). (b) Powder X-ray diffraction patterns acquired on **2**$_{DMF}$ as a function of the temperature in the temperature range 303-683 K, with steps of 20 K.

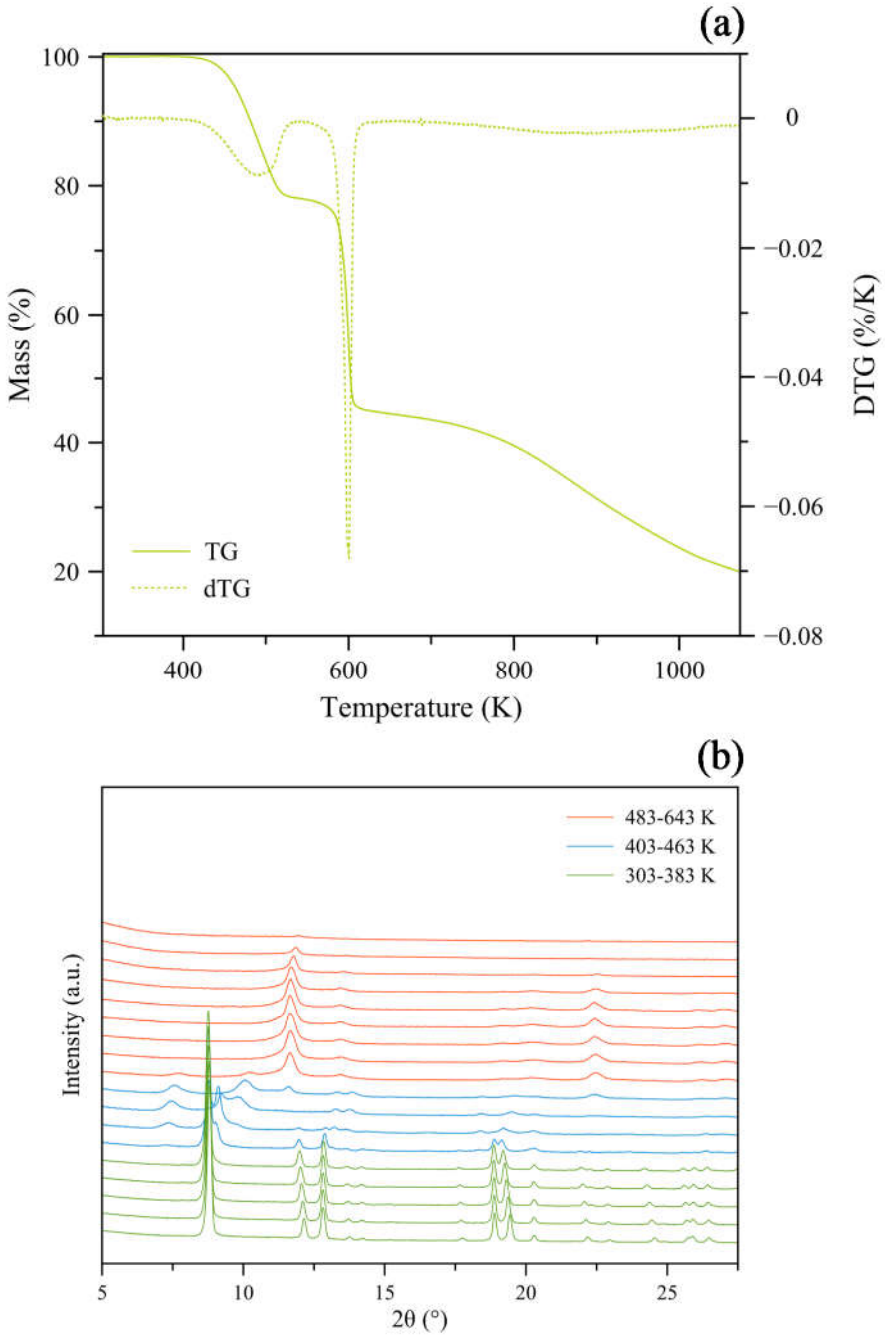

Figure S12. (a) TGA trace (green continuous line) measured under a flow of N_2 on **3**$_{DMF}$ and the corresponding DTG trace (green dashed line). (b) Powder X-ray diffraction patterns acquired on **3**$_{DMF}$ as a function of the temperature in the temperature range 303-643 K, with steps of 20 K.

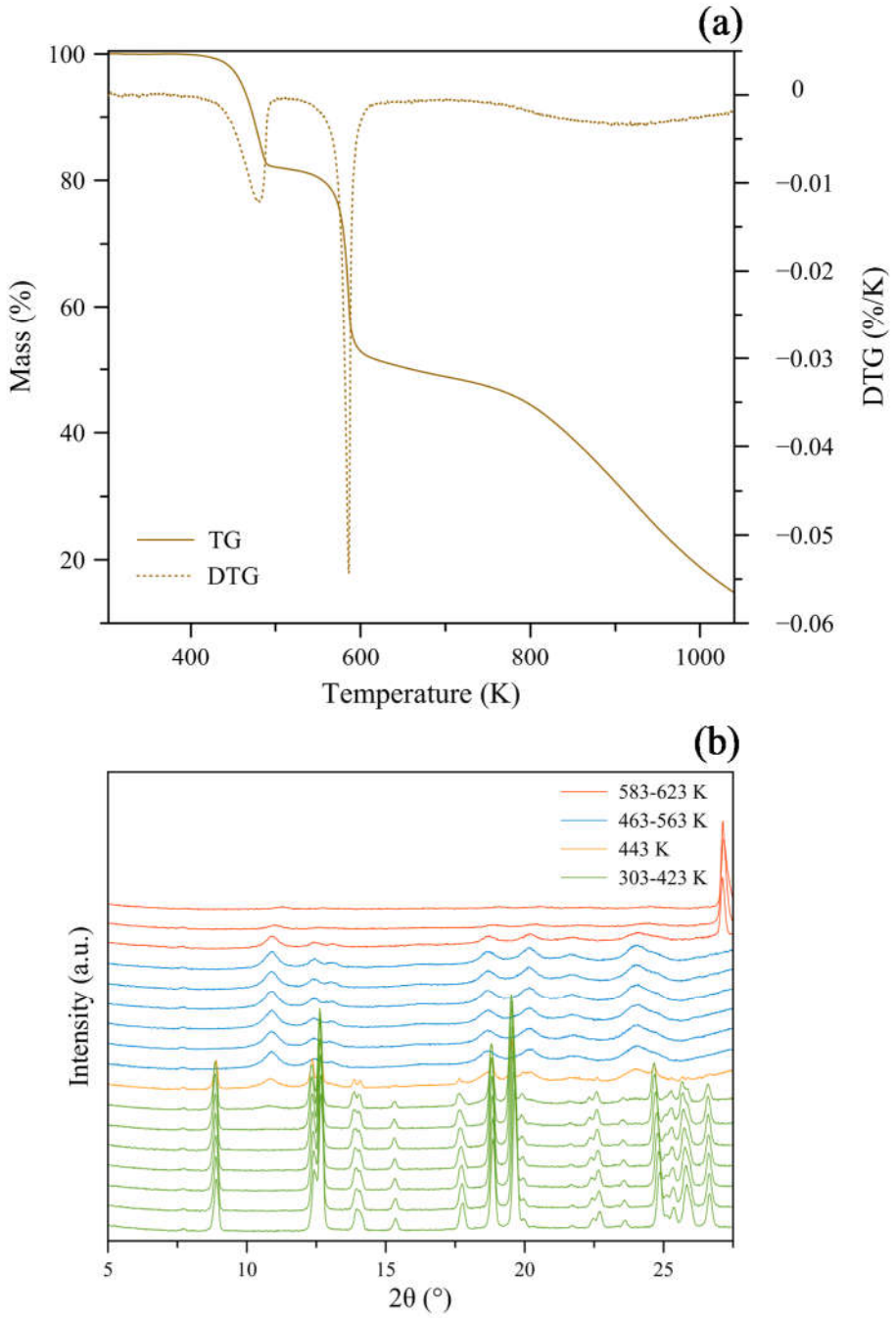

Figure S13. (a) TGA trace (brown continuous line) measured under a flow of N_2 on **4**$_{DMF}$ and the corresponding DTG trace (brown dashed line). (b) Powder X-ray diffraction patterns acquired on **4**$_{DMF}$ as a function of the temperature in the temperature range 303-623 K, with steps of 20 K.

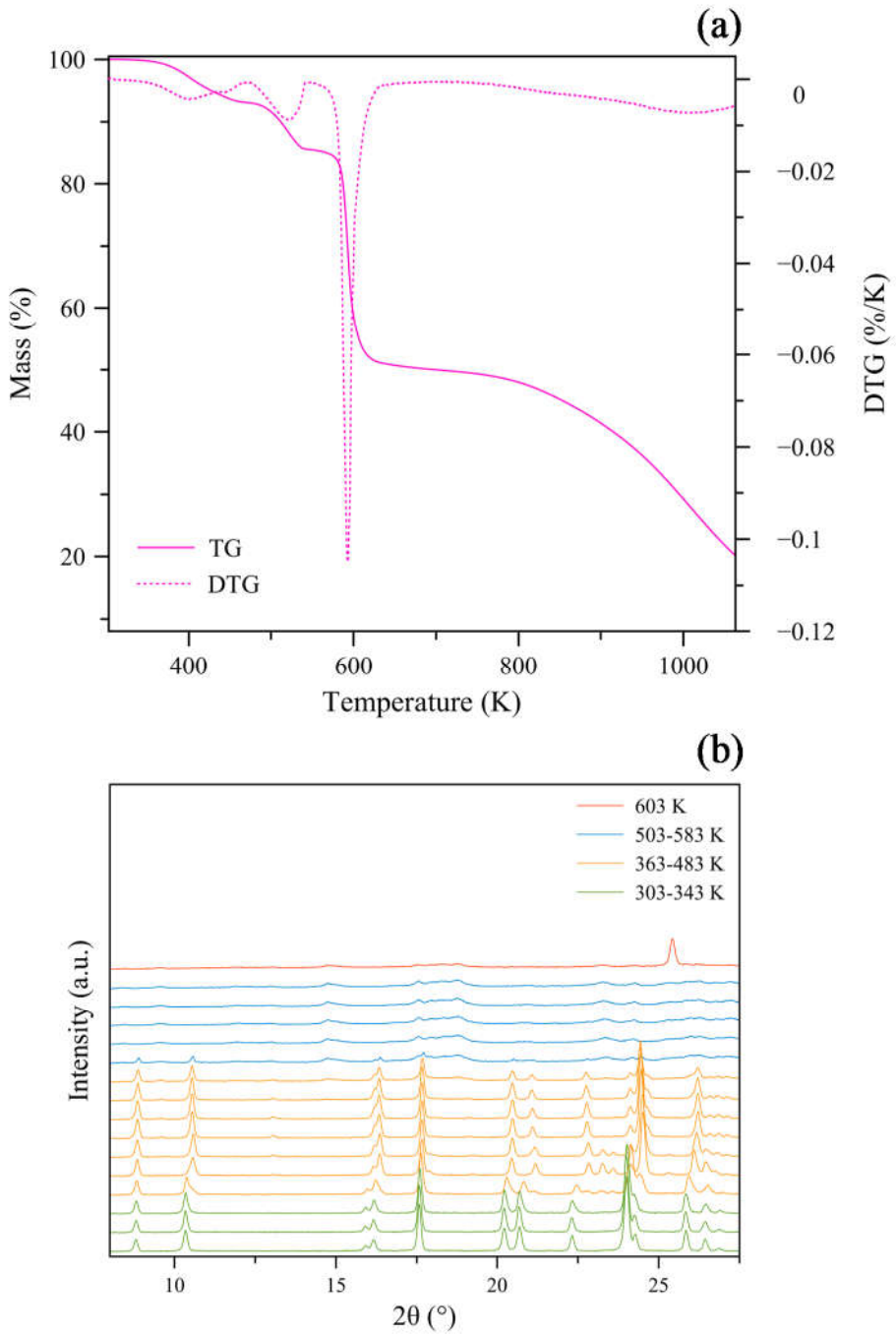

Figure S14. (a) TGA trace (purple continuous line) measured under a flow of N_2 on **5**$_{DMF}$ and the corresponding DTG trace (purple dashed line). (b) Powder X-ray diffraction patterns acquired on **5**$_{DMF}$ as a function of the temperature in the temperature range 303-603 K, with steps of 20 K.

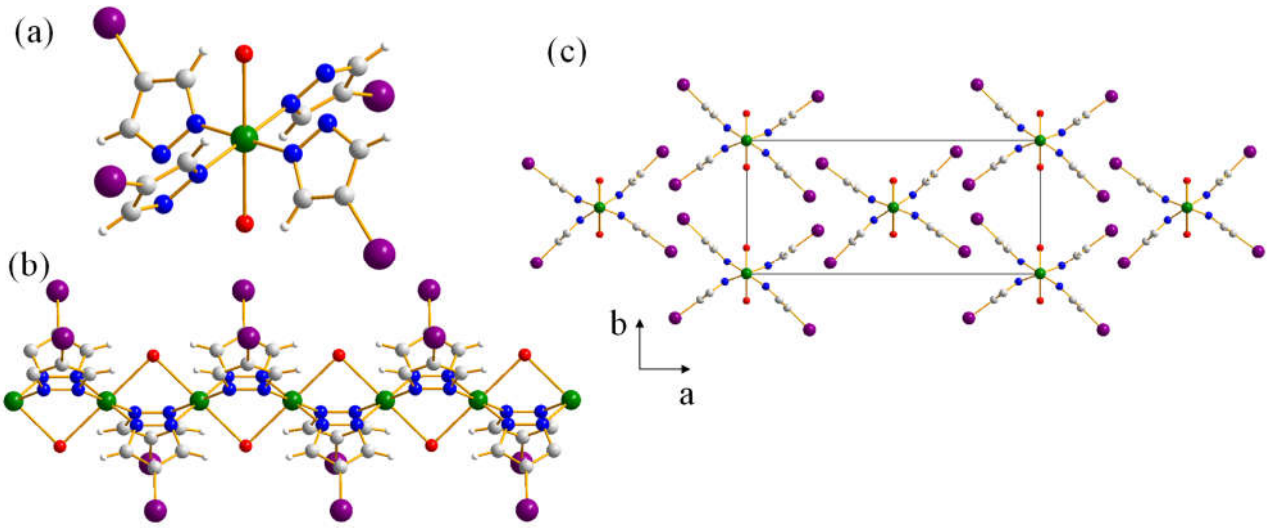

Figure S15. (a) Representation of the *trans*-CuN_4O_2 octahedral stereochemistry of the copper(II) ion in **oP-5$_{DMF}$**. (b) Representation of portion of the 1-D helix of collinear metal ions running along the [001] crystallographic direction in **oP-5$_{DMF}$**. (c) Representation of portion of the crystal packing of **oP-5$_{DMF}$** viewed along the [001] crystallographic direction. Horizontal axis, *a*; vertical axis *b*. Only the oxygen atoms of the DMF molecules have been depicted for clarity. Colour code: Carbon, grey; hydrogen, light grey; copper, green; iodine, violet; nitrogen, blue; oxygen, red. Main bond distances (Å) and angles (°) at the metal ion: Cu-N 1.9506(76), 1.9529(72); Cu-O 2.597(15); intra-chain Cu···Cu 3.6456(1); N-Cu-N 180; O-Cu-O 180; N-Cu-O 77.77(24) - 102.23(24).

Table S2. Optimized unit cell parameters computed at the B3LYP-D* level for the low-spin state compounds **1**-**oC-5$_{DMF}$**. Percentages in parenthesis is % ΔV with respect to the experimental value.

	1	**2$_{DMF}$**	**3$_{DMF}$**	**4$_{DMF}$**	**oC-5$_{DMF}$**
***a* (Å)**	17.7609	11.9212	13.5388	13.9300	18.7006
***b* (Å)**	6.7896	12.9050	13.6471	13.8518	9.3850
***c* (Å)**	6.5909	7.05378	7.04702	7.05687	7.5452
V (Å^3)	793.4 (-9%)	1085.1 (-9%)	1302.1 (-	1361.7 (-6%)	1324.2 (-7%)

Table S3. Optimized unit cell parameters computed at the B3LYP-D* level for the high-spin state compounds **1**-**oC-5**$_{DMF}$. Percentages in parenthesis is % ΔV with respect to the experimental value.

	1	**2**$_{DMF}$	**3**$_{DMF}$	**4**$_{DMF}$	**oC-5**$_{DMF}$
a **(Å)**	17.73575	11.99516	13.53887	13.93007	18.4346
b **(Å)**	6.79271	12.79345	13.64717	13.85183	9.2473
c **(Å)**	6.55168	7.12789	7.047021	7.05687	7.5566
γ **(°)**	90.0	90.0	90.0	90.0	87.9
V (Å^3)	789.3 (-9%)	1093.8 (-8%)	1302.1 (-	1361.7 (-6%)	1286.4(-

Table S4. Optimized unit cell parameters computed at the PBE level for the high-spin state compounds **1**-**oC-5**$_{DMF}$. Percentages in parenthesis is % ΔV with respect to the experimental value.

	1	**2**$_{DMF}$	**3**$_{DMF}$	**4**$_{DMF}$	**oC-5**$_{DMF}$
a **(Å)**	18.29387	12.8687	13.2282	14.86124	18.4792
b **(Å)**	6.8668	14.25077	16.42888	14.83259	10.0752
c **(Å)**	8.15015	7.28236	7.28364	7.2509	7.8170
γ **(°)**	90.0	90.0	90.0	90.0	90.2
V (Å^3)	1023.8	1335.5 (+12%)	1582.9	1598.3	1455.4

Table S5. Optimized unit cell parameters computed at the B3LYP-D* level for the hypothetical compounds **3**$_{CALC}$-**5**$_{CALC}$. Percentages in parenthesis refer to variations with respect to the corresponding compounds **3**$_{DMF}$-**5**$_{DMF}$.

	3$_{CALC}$	**4**$_{CALC}$	**5**$_{CALC}$
a **(Å)**	7.0799 (-	7.502 (-47%)	20.4477
b **(Å)**	15.256	15.000 (+8%)	6.6439 (-
c **(Å)**	7.5970 (+8%)	7.7445	7.7553 (≈
β **(°)**	90.0	90.0	100.5
V (Å^3)	820.6 (-40%)	871.5 (-36%)	1035.8 (-

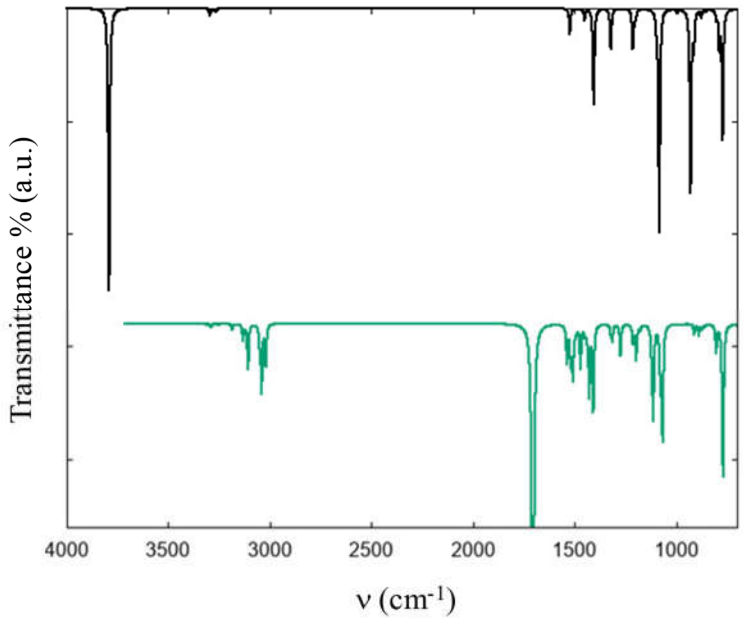

Figure S16. Computed IR spectra of [Cu(μ-pz)(μ-OH)]$_n$ (**1**, black) and [Cu(μ-pz)$_2$(μ-DMF)]$_n$ (**2**$_{\mathbf{DMF}}$, green).

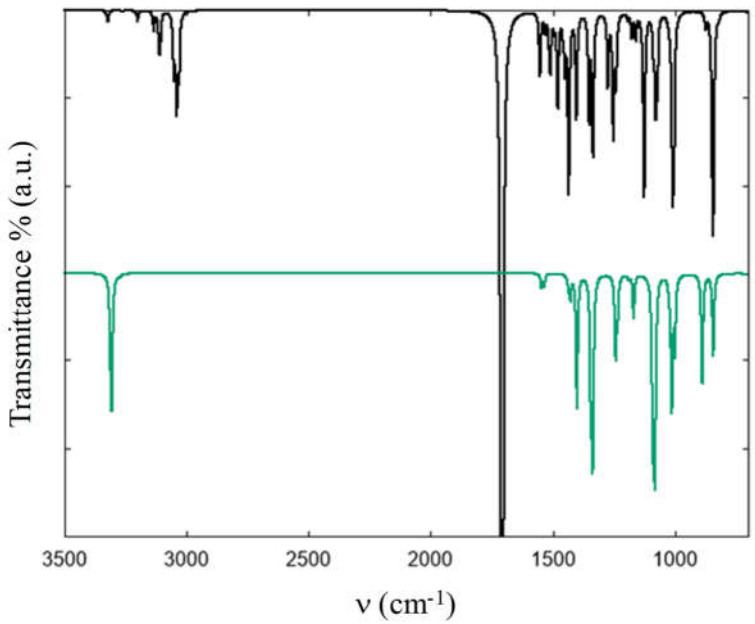

Figure S17. Computed IR spectra of [Cu(μ-4-Clpz)$_2$(μ-DMF)]$_n$ (**3**$_{\mathbf{DMF}}$, black) and [Cu(μ-4-Clpz)$_2$]$_n$ (**3**$_{\mathbf{CALC}}$, green).

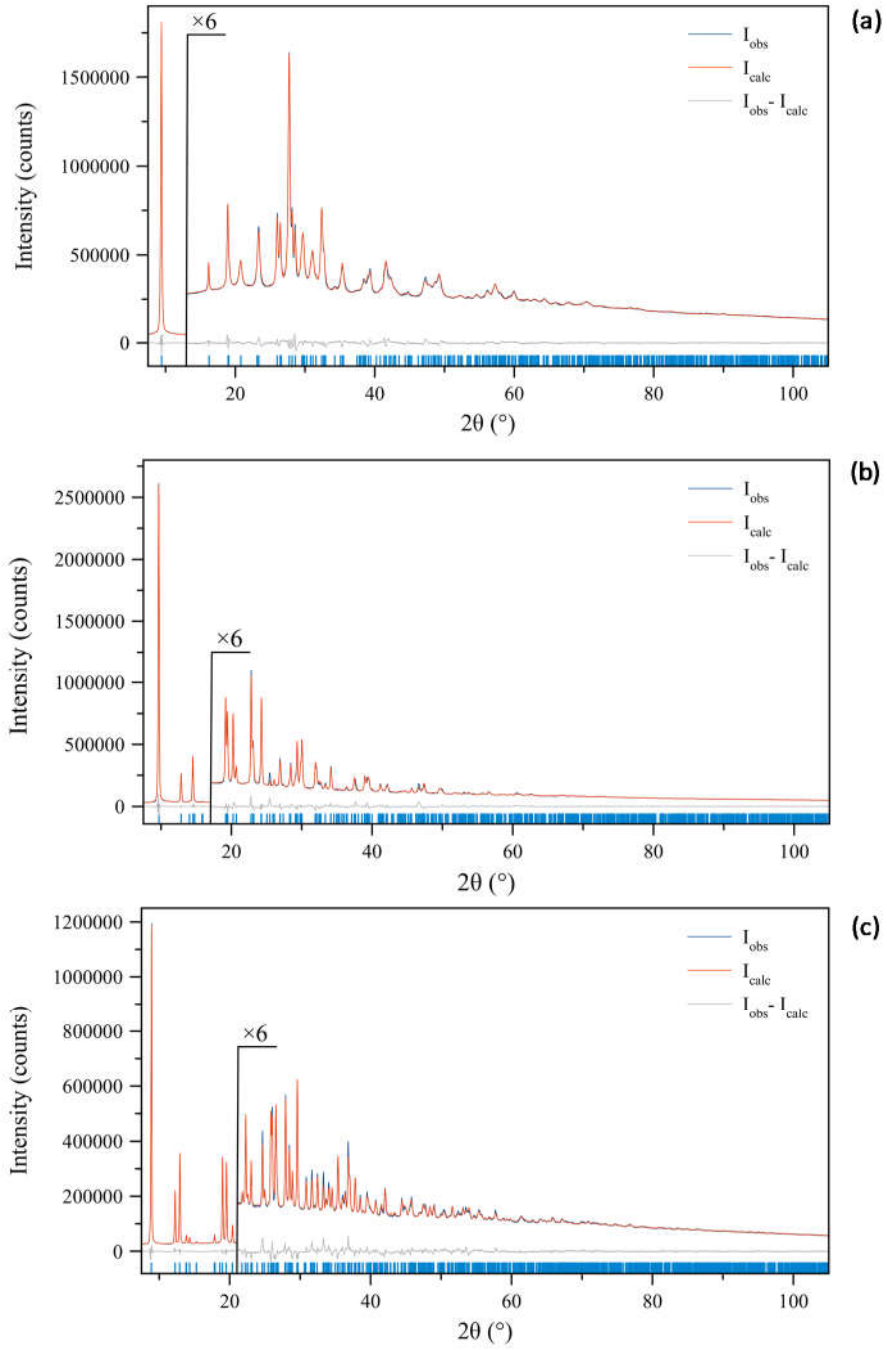

Figure S18. Graphical result of the final Rietveld refinements carried out on (a) **1**, (b) **2**$_{DMF}$ and (c) **3**$_{DMF}$ in terms of experimental, calculated and difference traces (blue, red and grey, respectively). The blue markers at the bottom indicate the positions of the Bragg reflections. Horizontal axis, 2θ (deg); vertical axis, intensity (counts).

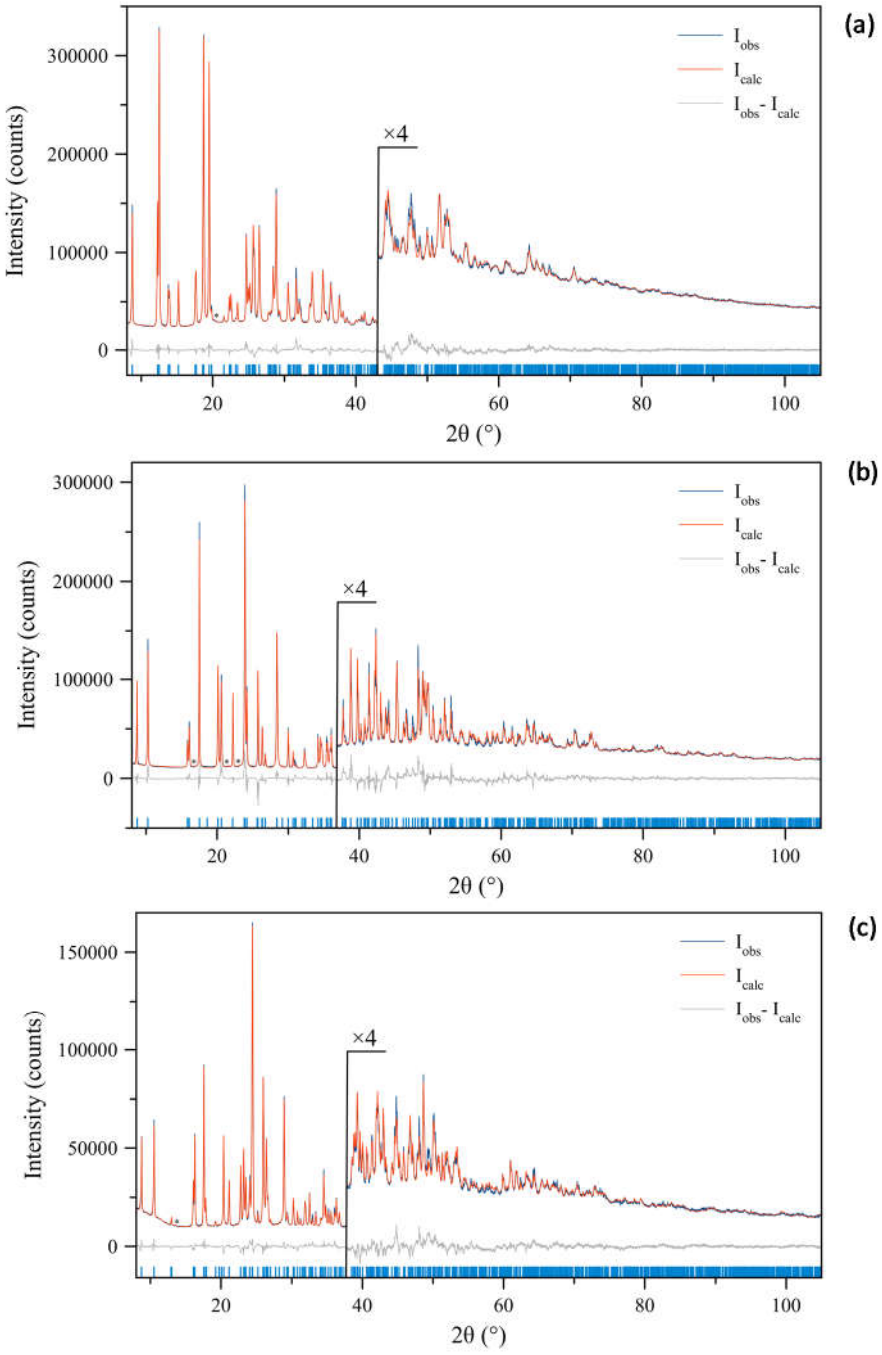

Figure S19. Graphical result of the final Rietveld refinements carried out on (a) **4**$_{DMF}$, (b) **oC-5**$_{DMF}$ and (c) **oP-5**$_{DMF}$ in terms of experimental, calculated and difference traces (blue, red and grey, respectively). The blue markers at the bottom indicate the positions of the Bragg reflections. Horizontal axis, 2θ (deg); vertical axis, intensity (counts). The asterisks indicate peaks belonging to impurities.

References

[1] A. Bondi, J. Phys.Chem. 1964, 68, 3, 441–451.

[2] C. J. E. Kempster and H. Lipson, Acta Cryst., 1972, B28, 3674.